Journal of Alloys and Compounds 954 (2023) 170106

Contents lists available at ScienceDirect

Journal of Alloys and Compounds

journal homepage: www.elsevier.com/locate/jalcom

NTO laminated graphite felt as high-performance negative electrode for vanadium redox flow batteries

Wen-Fei Liu [1], Kue-Ho Kim [1], Hyo-Jin Ahn *

Department of Materials Science and Engineering, Seoul National University of Science and Technology, Seoul 01811, South Korea

ARTICLE INFO

Article history:
Received 16 February 2023
Received in revised form 31 March 2023
Accepted 11 April 2023
Available online 12 April 2023

Keywords:
Vanadium redox flow battery
Anode
Composite
Graphite felt
Nb-doped TiO_2

ABSTRACT

In recent years, vanadium redox flow batteries (VRFBs) have attracted global interests owing to their advantages of large scale, high safety and long-term cyclability. Nevertheless, the unsatisfactory kinetics of carbon-based anodes limits the commercial application of VRFBs. Especially, graphite felt (GF) as a representative anode material, has critical disadvantage of poor electrolyte wettability due to its hydrophobic surface. This limitation of interfacial properties between the electrode and electrolyte causes inefficient charge transportation, which leads to low electrochemical performance with poor cycle stability. To improve the surface properties of GF anodes for VRFB, we introduce a lamination layer of Nb-doped TiO_2 (NTO) to a heat-treated graphite felt (HGF) via ultrasonic spray pyrolysis deposition. The NTO laminated HGF offers hydrophilic surface with several advantages of high catalytic activity, high electrical conductivity, and high specific surface area. As an anode material, the hybrid structure of the NTO lamination layer on the HGF demonstrates synergistic effects, thus enabling superior energy storage performance compared with other electrodes. Especially, the NTO-HGF anode shows an energy efficiency of 82.03%, which is 6.2% higher than that of pristine GF. We demonstrate that the introduction of an NTO lamination layer can be a prospective candidate for improving the VRFB anodes performance.

1. Introduction

The continually increasing global energy consumption has accelerated the demand for sustainable energy sources. The growth of rechargeable energy storage market, including redox flow batteries, fuel cells, and lithium-ion batteries has received significant attention as restrictions on fossil fuels have increased. Therefore, the performance of electrochemical energy storage technology must be enhanced to solve future energy problems [1–3]. Electrochemical energy storage devices possess key advantages of high efficiency, eco-friendliness, and controllable energy densities. To date, various types of flow batteries have been developed, such as iron–chromium flow batteries, zinc–bromine flow batteries, and vanadium redox flow batteries [4–6] owing to their long-term cyclability.

Especially, the vanadium flow battery (VRFB), which is known as prominent candidate for next-generation energy storage system. VRFBs possess several advantages, including flexible capacity design, high safety, high efficiency, and long cycle life [7]. By adjusting the amount of electrolyte, the capacity of a VRFB can be easily controlled depending on the application type. Additionally, VRFBs system alleviate cross-contamination problems owing to the vanadium chemical utilization in both the anolyte and catholyte of the cell (V^{2+} /V^{3+} solution for the anolyte, and VO_2^+ /VO^{2+} solution for the catholyte) [8]. As the application fields of large-scale energy storage system, VRFBs rapidly substitutes conventional Li-ion batteries owing to their non-flammability and long-term cyclability with beneficial levelized cost of electricity (LCOE). These advantages facilitate the commercialization of VRFBs market, together with the development of related techniques. Several key concepts have reported for designing high-performance electrode materials such as constructing composite materials and morphology control [9–13]. However, during the redox process, electrode material do not participate for chemical reaction, which is a distinct characteristic of VRFB compared with other secondary battery systems. The electrode material offers reaction sites during charge/discharge process and transports charge carriers to the redox couples, which can contribute to the overall energy storage performance, such as energy density and efficiencies. Therefore, to enhance the energy-storage performance of VRFBs, electrode materials must possess high porosity, mechanical and chemical stability, and high electrical conductivity. Graphite felt (GF) is a representative electrode material owing to its

* Corresponding author.
E-mail address: hjahn@seoultech.ac.kr (H.-J. Ahn).
[1] Wen-Fei Liu and Kue-Ho Kim contributed equally to this work.

https://doi.org/10.1016/j.jallcom.2023.170106
0925-8388/

high porosity, great electronic conductivity, low cost, and superior electrochemical stability [14–16]. The morphology of the electrode material affect the kinetic properties during electrochemical reactions that occur at the surface of the electrode. Moreover, the wettability of the electrolyte on the electrode material dominantly affects the efficiency of the VRFB, which determines the quality of interfacial contact [17]. However, GF electrodes are hydrophobic and exhibits unsatisfactory catalytic activity for vanadium redox reactions. Hence, several strategies have been investigated to modify the intrinsic characteristics of GF. One of the modification strategies, developing heteroatom-doped GF can effectively increase the electrical conductivity, providing additional charge carrier [18–21]. Through the doping methods, surface characteristics including wettability can be modified owing to the introduction of additional functional group. On the other hands, constructing hybrid composite materials considered a powerful strategy, which can compensate the critical disadvantages of GF. Representatively, Pt, Ir, Au, and Ru were coated onto the surface of GF for accelerating the reaction of the redox couple owing to their excellent electrochemical activity and high electrical conductivity [22–26]. However, using precious metals incurs a high cost, which renders them unsuitable for designing practical VRFB systems. Moreover, metal oxides such as TiO_2 and Mn_3O_4 exhibit intrinsically low electrical conductivities. These limitations hinder their application to VRFB systems [18,27]. Therefore, the development of novel catalysts with high electrochemical activity, large specific surface area, high conductivity, and affordable cost is urgently required to facilitate the commercialization of VRFBs.

Herein, Nb-doped TiO_2 lamination layer-covered heat treated GF (NTO-HGF) for a high-efficiency VRFB anode using fabrication via a simple and low-cost horizontal ultrasonic spray pyrolysis deposition (HUSPD) is proposed. Surface NTO layer successfully enhanced the electrical conductivity and catalytic activity of GF. The resultant NTO-HGF sample exhibited excellent electrocatalytic performance with superior electrolyte wettability, resulted in high EE and enhanced cycle stability when it was used in the VRFB anode.

2. Experimental

First, the GF(4.7 mm thickness, Mirfa) was cleaned ultrasonically using ethanol and deionized water at a ratio of 1:3 for 30 min. Subsequently, the GF was washed with deionized water for 10 min. After cleaning, the GF was dried at 80 °C for 12 h. To increase surface area and electrochemical activity, the dried GF was heat treated in an air atmosphere box furnace at 420 °C for 10 h, and the sample was labeled as HGF. As shown in Fig. 1, HUSPD was used to prepare a NTO lamination layer covered with HGF. The following procedure was used to prepare the precursor solutions: First, 2.025 g of niobium chloride ($NbCl_5$, Sigma, > 99%) was dissolved in 300 mL of ethanol and stirred for 2 h. Subsequently, 9 mL of diisopropoxide titanium ($C_{16}H_{28}O_6Ti$, Alfa Aesar, 75% in isopropanol) solution was added and stirred for another 2 h. For the HUSPD process, the HGF was placed on a cleaned glass holder, and an ultrasonically atomized (1.6 MHz) precursor solution was thermally deposited on HGF substrate in a heating chamber at 420 °C. NTO particles were deposited on the HGF substrate for 60 min using air as a carrier gas at flow rate of 15 L/min and a fixed rotation speed of the holder at 5 rpm, and the sample was labeled as NTO-HGF. All other conditions were used to minimize error, and the sample fabricated without niobium chloride in the precursor solution was labeled TiO_2-HGF.

To figure out the morphology and composition, field-emission scanning electron microscopy (FESEM) was conducted with. Crystallographic and chemical bonding states were analyzed using X-ray diffraction (XRD) and X-ray photoelectron spectroscopy (XPS, K–ALPHA$^+$). To investigate the wettability, interfacial characteristic between the prepared graphite felts and electrolyte (0.15 M V^{3+} with 3 M H_2SO_4) was evaluated using contact anglemeter (KSV200). Cycle voltammetry and electrochemical impedance spectroscopy were performed using a prepared electrode. A silver chloride electrode (Ag/AgCl) and platinum sheet electrode were used as the reference and counter electrodes to proceed the three-electrode measurement system. The GF, HGF, TiO_2-HGF, and NTO-HGF were cut into circles (0.3 cm^2) for the measurement, and 0.15 M V^{3+} with 3 M H_2SO_4 solution was used as the electrolyte. The scan rate was set to 5 mV/s with a voltage window of − 0.8–0 V(vs. SCE) for V^{3+}/V^{2+} redox reactions. For the two-electrode full cell test, the GF was cut into rectangular samples measuring 20 mm × 30 mm with a Nafion 212 separator. The pristine GF electrode was used as the cathode side for all full-cell tests. On the anode side, GF, HGF, TiO_2-HGF, and NTO-HGF samples of the same size were successively used for testing and comparison. The 1.5 M vanadyl sulfate trihydrate ($VOSO_4{\cdot}3H_2O$, TCI, > 98%) dissolved in 3 M sulfuric acid (H_2SO_4, DUCSAN, > 98%) was used as an initial electrolytes for both anode and cathode. To exhaust oxygen in the electrolyte tank, the electrolyte was purged with Ar for 15 min. The initial discharge process was set to convert the catholyte and anolyte from VO^{2+} to VO_2^+ and V^{3+}, respectively. The voltage window was 1.6 V and 0.7 V for charge/discharge under different current densities ranging from 40 to 160 mA/cm^2. The charge/discharge cycle tests of the VRFB were performed using a battery cycler (WonATech, WBCS 3000 L).

3. Results and discussion

Fig. 2 displays the FESEM data obtained from the GF, HGF, TiO_2-HGF, and NTO-HGF samples. By adopting the HUSPD method, precursor droplets can be deposited onto the substrate more uniformly, owing to the indirect droplet-supplying mechanism featuring a rotating disk. Thus, a GF sample with a uniform NTO lamination layer was successfully developed, as depicted in the schematic images. As shown in Fig. 2(a) and (e), a smooth morphology was observed on the surface of the GF with an average felt diameter of ~14 µm, which is not a favorable structure owing to the low specific surface area [28]. After the heat treatment, the surface exhibited a rough and porous structure, as shown in Fig. 2(b) and (f), which provided sufficient active sites for the redox reaction and facilitated the growth of the NTO lamination layer [29]. Fig. 2(c) and (g) show the FESEM images of TiO_2-HGF, indicating that TiO_2 particles were synthesized on the HGF surface via the HUSPD method. The presence of dense and rough surface nanoparticles, as shown in Fig. 2(d) and (h), proves that the NTO particles were uniformly distributed on the HGF surface, which consequently increased the surface roughness of the HGF. The NTO lamination thickness confirmed as approximately 32 nm, as shown in Fig. S1. In addition, an EDS analysis was performed to verify the constituent elements (Fig. 2i). The EDS data confirmed the uniform distribution of Ti and Nb, signifying a well-laminated NTO layer on the HGF.

In the XRD pattern, owing to the thin lamination layer of NTO than the graphite felt substrate, the diffraction pattern of the NTO phase was included in the graphite phase (JCPDS# 41–1487) and was not distinguishable, as shown in Fig. S2 [30,31]. Fig. 3(a) shows the full-range XPS data obtained from the GF and NTO-HGF, including the O KLL, O 1 s, Ti 2p, C 1 s, and Nb 3d peaks. To investigate the detailed peaks of each bond, magnified XPS data of the NTO-HGF samples are shown in Fig. 3(b–e). In Fig. 3(b), the NTO-HGF maintained the carbon-related bonding states of GF, including C═C, C–C, C–O, and C═O at ~284.6, 285.1, 286.0, and ~287.7 eV, respectively. This shows that the heat treatment and HUSPD processes did not excessively oxidize carbon but maintained the graphite felt structure. The oxygen-related functional groups in Fig. 3(c) show the OH phase, C═O bonds, and H–O–H bonds in the fitted peaks at ~532.6, 531.0, and ~534.2 eV, respectively. This oxygen-related functional group can contribute to the wettability of the acid-base electrolyte

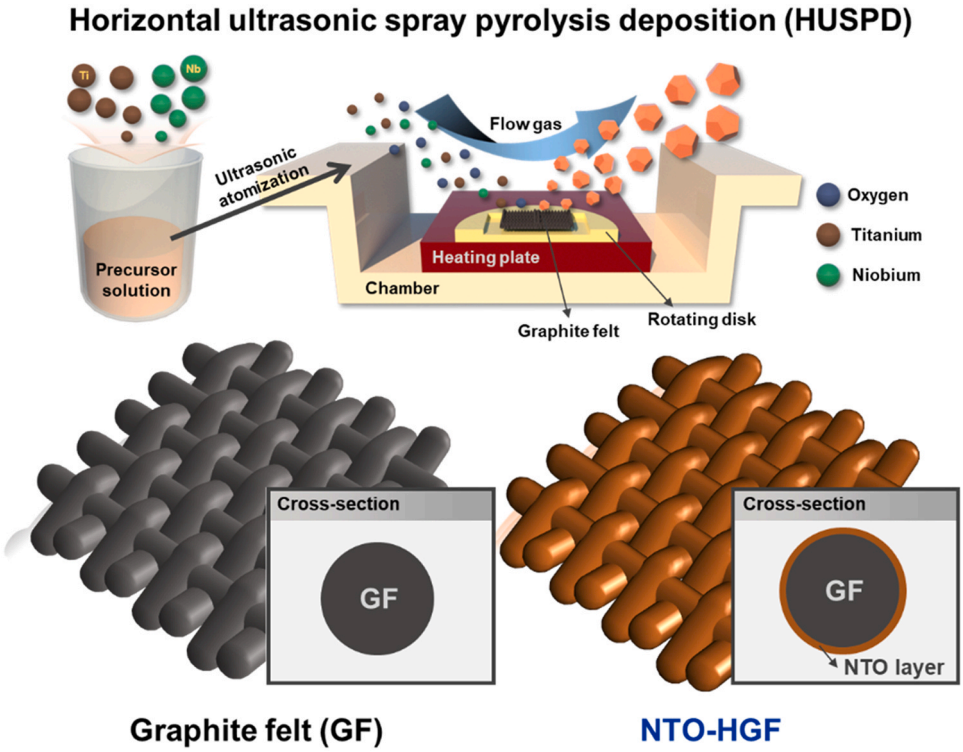

Fig. 1. Schematic diagram of the process of synthesizing NTO on HGF using HUSPD.

on the electrode, which can enhance the energy storage efficiency during cycling. Fig. 3(d) appears the binding energy of the Ti 2p XPS spectrum. The two main peaks of Ti 2p at ~458.4 and ~464.1 eV, implying the Ti $2p_{1/2}$ and Ti $2p_{3/2}$ peaks, respectively, which imply the Ti^{4+} oxidation state relative to the TiO_2 phase. In addition, this sample show two secondary peaks at ~456.7 and ~462.5 eV, which indicates the Ti^{3+} oxidation state generated by the substitution of Ti^{4+} ions by Nb^{5+} ions. These substituted Nb^{5+} ions offer additional charge carriers to the lattice of TiO_2, which can contribute to the high electrical conductivity of NTO. The Nb 3d XPS core-level spectra (Fig. 3e) show that Nb $3d_{5/2}$ emitted a main peak at ~206.6 eV and Nb 3d $_{3/2}$ at ~210.0 eV, which indicates the presence of Nb^{5+}. Meanwhile, the secondary peaks, which appeared at ~205.8 and ~209.1 eV for Nb $3d_{5/2}$ and Nb $3d_{5/2}$, respectively, indicate the coupling peaks of Nb atoms doped on the TiO_2 lattice. Thus, the NTO lamination layer was successfully synthesized via the HUSPD process [32,33]. To confirm the wettability of GF, HGF, and NTO-HGF, 5 μL of sulfuric acid-based vanadium electrolyte (0.15 M V^{3+} with

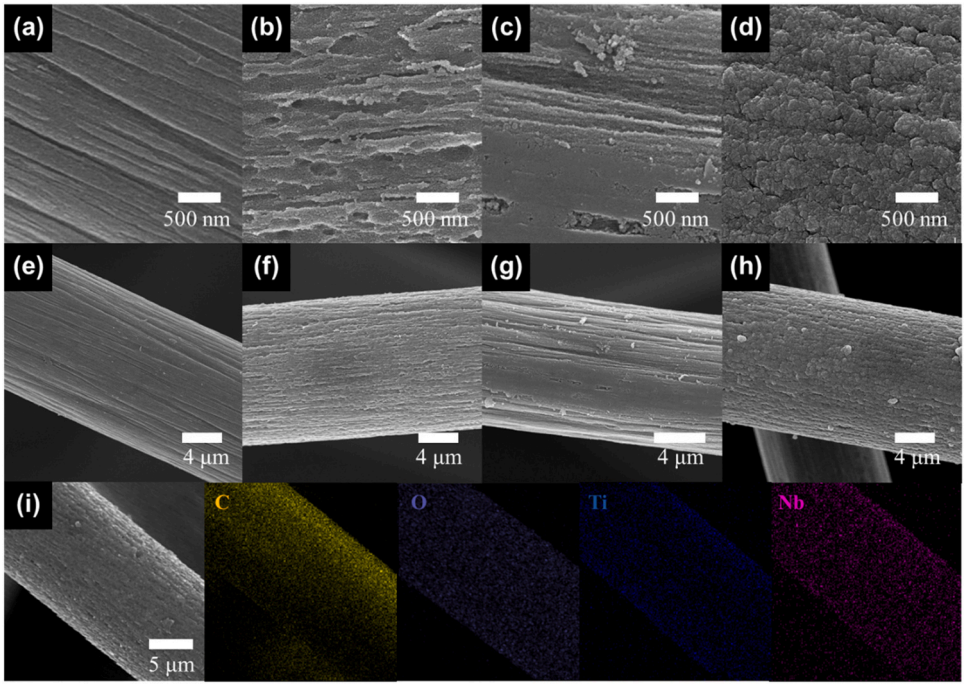

Fig. 2. (a–h) HRSEM images of GF, HGF, TiO_2-HGF, and NTO-HGF samples and NTO-HGF with (i) EDS mapping data of NTO-HGF.

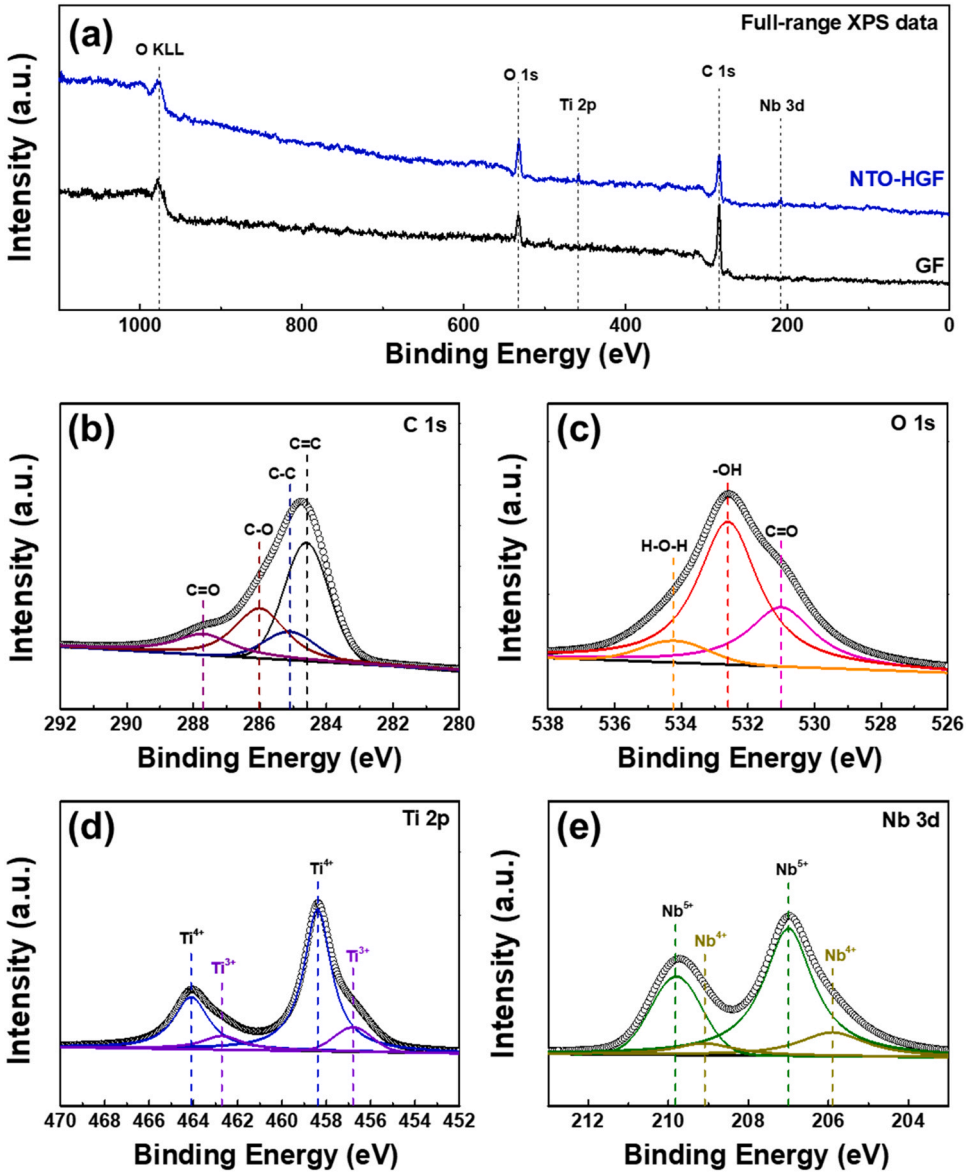

Fig. 3. (a) Full-range XPS data obtained from GF and NTO-HGF, and magnified specific (b) C 1 s, (c) O 1 s, (d) Ti 2p, and (e) Nb 3d XPS data of NTO-HGF.

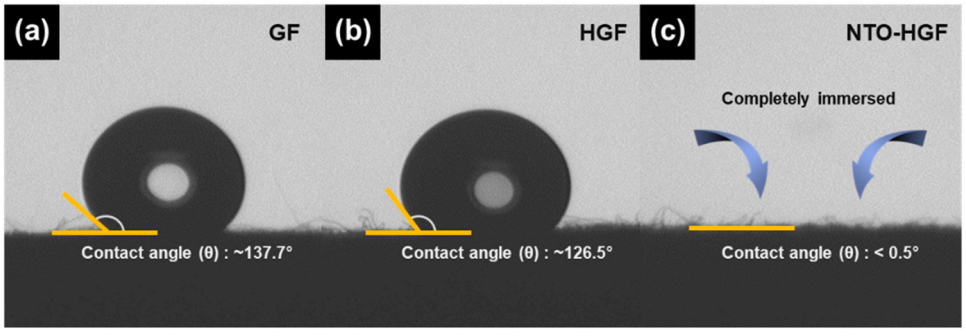

Fig. 4. Contact angle data between sulfuric acid-based vanadium electrolyte drop and (a) GF, (b) HGF, and (c) NTO-HGF.

3 M H_2SO_4) was drop onto all the samples, respectively (Fig. S3). In Fig. 4, the contact angle between the electrode and electrolyte was measured using contact anglemeter. GF and HGF shows high contact angle of ~137.7° and ~126.5° owing to its strong hydrophobic surface property. This poor wettability of GF and HGF electrodes can causes inefficient charge transfer during the continuous charge/discharge process accompanied with the restricted reaction sites. Interestingly, NTO-HGF electrode completely absorbed the electrolyte (contact angle < 0.5°), signifying the superior wettability compared with other samples. The excellent wettability was mainly attributed to the abundant oxygen-related functional groups at the surface of NTO

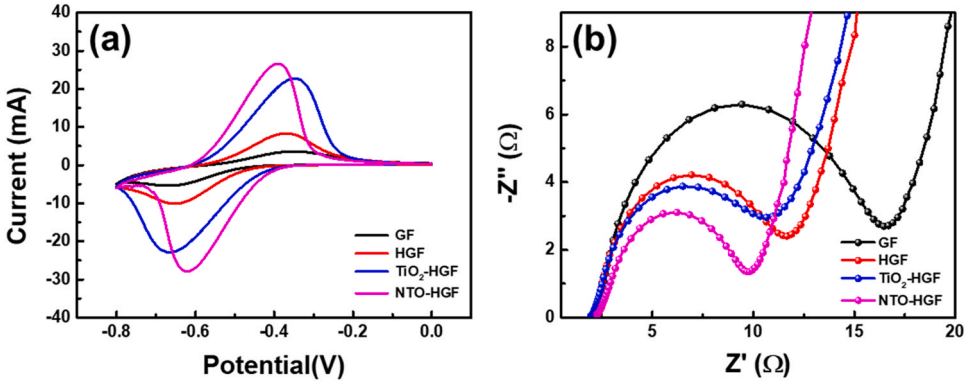

Fig. 5. (a)The CV curves at a scan rate of 5 mV/s and (b) EIS curves of various electrodes in 0.15 mol L^{-1} $VOSO_4$ + 3 mol L^{-1} H_2SO_4 solution.

lamination layer, which provides sufficient active sites with stable long-cycle stability of VRFBs [34].

CV measurements were conducted for the GF, HGF, TiO_2-HGF, and NTO-HGF electrodes to estimate their electrochemical activities toward the electrochemical coupling reaction. Fig. 5(a) exhibits the anodic CV data for all electrodes at a scan rate of 5 mV/s. The peak current and peak current differences were used to evaluate the electrochemical activity of the electrode materials via CV [35,36]. The TiO_2 and NTO lamination layer covered electrodes show enhanced electrochemical characteristics such as increased redox current with lower peak potential separation (ΔE_p) compared with the HGF and GF electrodes. This is because the presence of TiO_2 enhances the adsorption of V^{3+} ions and provides more reactive sites owing to the presence of –OH, thus promoting the electrochemical reaction of V^{3+}/V^{2+} [37]. The NTO-HGF electrode exhibited the highest redox peak current density (J_{pc}) and ΔE_p during the V^{3+}/V^{2+} reaction, indicating the high reversibility and enhanced electrochemical activity of the NTO-HGF electrode for the V^{3+}/V^{2+} reaction. This result demonstrates the significantly enhanced electrochemical characteristics of the NTO-HGF electrode by applying the NTO lamination layer caused by the enhanced surface area with the high electrocatalytic activity of NTO and the presence of Nb atoms, which improved the conductivity of TiO_2.

The electrocatalytic activity of all the electrodes for the V^{3+}/V^{2+} reaction was further investigated via EIS. Fig. 5(b) shows Nyquist plots for the GF, HGF, TiO_2-HGF, and NTO-HGF. The EIS profile (Nyquist diagram) generally comprises two regions: a semicircular region and a straight-line region. The semicircle diameter of the Nyquist diagram indicates the charge-transfer resistance (R_{ct}), which represents the interfacial resistance within the cell [38]. This interfacial resistance can affect the V^{3+}/V^{2+} redox reaction on the anode side during the charge/discharge cycles. Consequently, the NTO-HGF electrode exhibited the smallest semicircle diameter, signifying the highest electrical conductivity, which is well-matched with the result of CV test. The combined CV and EIS data exhibit that the NTO-HGF electrode exhibited great redox activity for V^{3+}/V^{2+}. Because the NTO-HGF electrode accommodates a more reversible redox pair with lower resistance, it can be used as an electrode to improve the energy conversion efficiency of VRFB anodes.

To further investigate the kinetic properties of the NTO-HGF during the V^{3+}/V^{2+} reaction, CV tests were performed for the NTO-HGF and GF under different scan rates, as shown in Fig. 6(a) and (b). At all scan rates, the NTO-HGF showed enhanced current values and lower peak potential differences compared with the HGF. Using Randles–Sevcik equation [39], the mass transfer rate of vanadium ion coupling was investigated. Fig. 6(c) shows a plot of the peak current density vs. the square root of the scan rate for the GF and NTO-HGF anodes. The peak currents at both the GF and HGF anodes are proportional to the square root of the scan rate, signifying diffusion-controlled V^{3+}/V^{2+} reaction at both electrodes [40]. The straight line slope for the NTO-HGF was higher than that for the GF, indicating that the mass transfer process at the surface of the NTO-HGF was faster than that at the GF surface. The enhanced mass transfer performance is owing to the increased number of active sites by heat treatment and the enhanced hydrophilicity of the electrodes by the uniform NTO lamination layer. Moreover, doped Nb^{5+} ions, which substitute Ti^{4+}, facilitate charge transfer during the redox reactions, thus providing additional charge carriers to the TiO_2 lattice.

For investigating the NTO lamination layer effect on the electrochemical performance of the electrode in detail, the GF, HGF, TiO_2-HGF, and NTO-HGF were loaded into a VRFB system, as shown in Fig. 7(a), and charged/discharged at a current density of 120 mA/cm^2 (Fig. 7(b)). The electrode modification effects on the VRFB performance was demonstrated. Compared with the VRFB with the GF anode, the VRFB with the NTO-HGF anode exhibited a lower charging voltage and a higher discharging voltage, indicating that the NTO-HGF became less polarized during the redox reaction. Moreover, the VRFB with the NTO-HGF anode showed the highest discharge capacity compared with the other electrodes, under the same amount of electrolyte. This was owing to the additional active sites of NTO-HGF electrode, which promoted the charge transfer of vanadium ions. This can in fact contribute to a higher voltage efficiency (VE), EE, and coulombic efficiency (CE). In Fig. 7(c–e), NTO-HGF anode exhibited the highest EE of 95.18% at a current density of 40 mA/cm^2. The high energy efficiency of the NTO-HGF is mainly attributed to the enhanced catalytic activity caused by the conductive NTO lamination layer, accompanied by abundant oxygen functional groups. During the cell operation, the reaction of the redox couple can be facilitated owing to the improved electrochemical catalytic property and additional reaction sites for NTO-HGF anode. Moreover, the NTO-HGF anode showed superior CE and VE among all the samples. Interestingly, the VE gap between the pristine GF and NTO-HGF widened gradually. This is because, at low current densities, the gap was not significant owing to the lower polarization of the VRFB cell. Under high current, the polarization for pristine GF increased, which rapidly degrades the VE. However, the reduced polarization of the NTO-HGF electrode from enhanced catalytic activity and additional active sites contributed to the VE retention rate, even under a high current density. The EE, CE, and VE of NTO-HGF were 6.2%, 3.2%, and 3.6% higher than GF at 160 mA/cm^2, respectively. These results show that the NTO-HGF possesses high electrocatalytic activity with sufficient active sites for redox reactions, particularly at high current densities. In addition, after cycling at a high current density of 160 mA/cm^2, the NTO-HGF electrode maintained its EE, CE, and VE when the current density was restored to 40 mA/cm^2, signifying high electrochemical stability in strongly acidic electrolytes [41]. Thus, the NTO-HGF exhibited superior

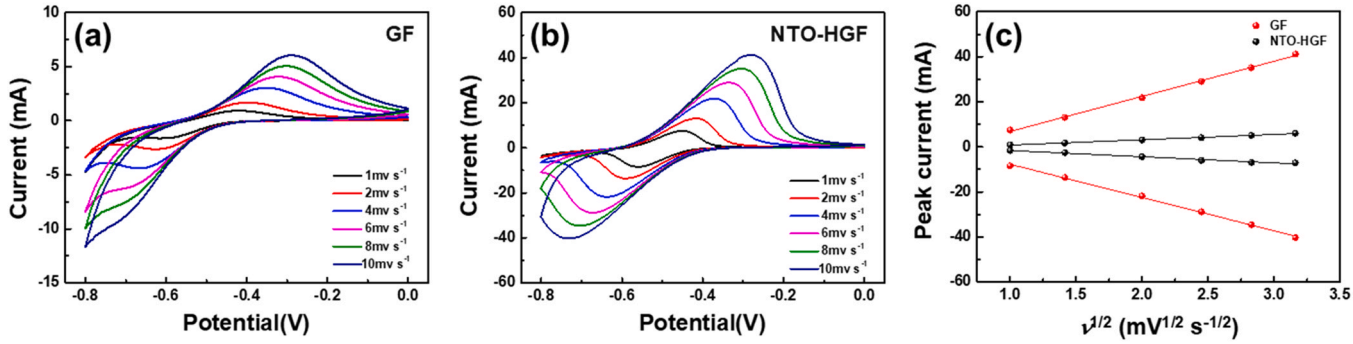

Fig. 6. CV curves of (a) bare GF and (b) NTO-HGF at different scan rates, obtained by using a negative electrolyte. (c) Plots of peak current density versus the square root of the scan rate for the V^{3+}/V^{2+} redox reaction.

electrochemical activity, which is mainly attributed to the enhancement in the oxygen-related functional groups and increased electrical conductivity [42]. The resultant NTO-HGF anode exhibited improved electrocatalytic activity and reduced electrochemical polarization of the VRFB cell. To further investigate the cycle stability of the GF and NTO-HGF, repetitive cycle tests were performed up to 100 cycles for the GF and NTO-HGF electrodes. As shown in Fig. 8(a). The discharge capacity of both cells decreased due to the precipitation of vanadium and ion diffusion through the membrane, which caused an imbalance of ion concentration in the anode and cathode sides of the VRFB cell [43]. However, after 100 cycles, the discharge capacity retention of the NTO-HGF was 67%, which was 17% higher than that of the cell with the GF electrodes. Moreover, as shown in Fig. 8(b), the NTO-HGF electrode exhibited a high and stable CE compared

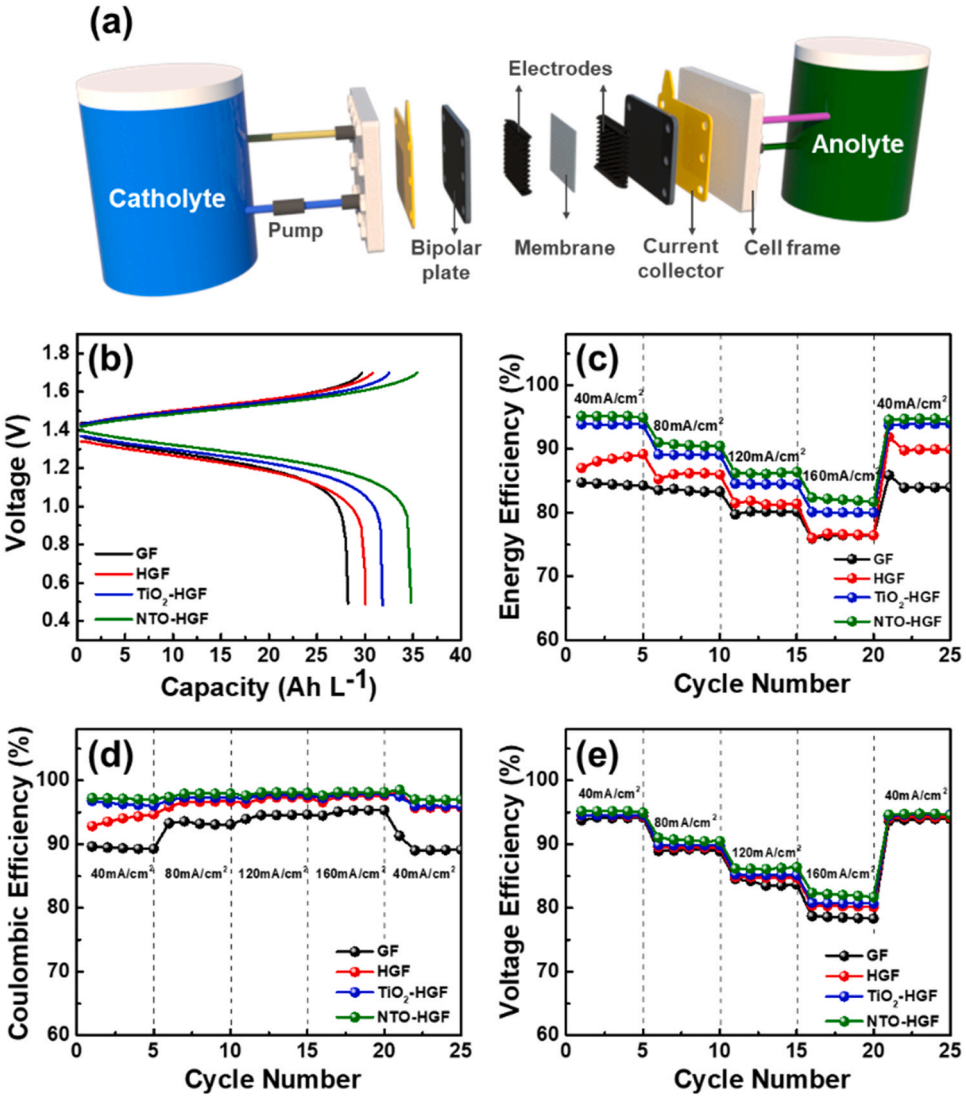

Fig. 7. (a) A schematic image of VRFB full cell evaluation system, (b) Charge–discharge curves of the GF, HGF, TiO_2-HGF, and NTO-HGF at a current density of 120 mA/cm^2, (c) energy, (d) coulombic, and (e) voltage efficiencies of the cells with the cycle number at current densities, 40–160 mA/cm^2.

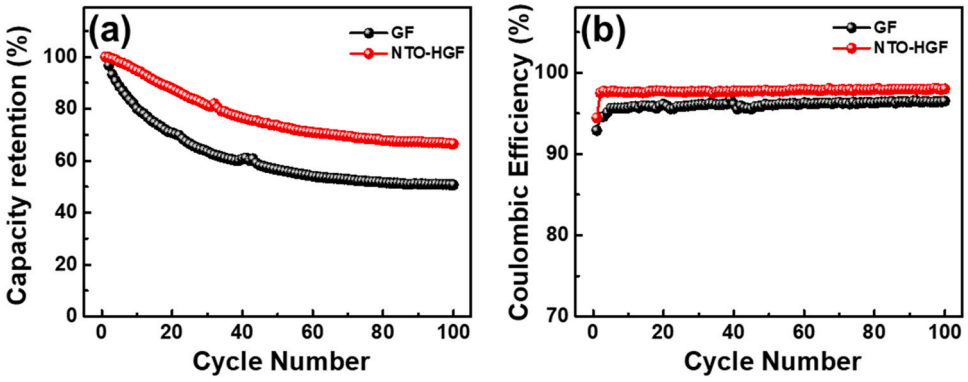

Fig. 8. (a) Discharge capacity retention and (b) coulombic efficiencies at a current density of 150 mA/cm^2 for 100 cycles.

with the pristine GF without significant degradation up to 100 cycles, which further reveals the superior stability of the NTO-HGF. The enhanced capacity retention of NTO-HGF was mainly attributed to the improved wettability from the surface NTO lamination layer, possessing additional oxygen-related functional groups. Consequently, the high VRFB anode performance of NTO-HGF sample is attributed to the following reasons. First, additional active sites were generated through the heat treatment of the pristine GF, which maximized the discharge capacity via a fixed electrolyte. Second, the oxygen-related functional groups of the NTO lamination layer increased the wettability of the NTO-HGF electrode, which resulted in superior cycle stability. Third, the enhanced electrical conductivity of the Nb-doped TiO_2 structure contributed to the energy storage efficiency during the charge/discharge process.

4. Conclusion

In summary, the NTO-HGF achieved via HUSPD exhibited outstanding electrochemical characteristics. The CV and EIS test results indicated that the NTO-HGF exhibited superior electrochemical activity. In addition, the NTO-HGF exhibited excellent electrochemical performance (highest EE of 95.18% at a current density of 40 mA/cm^2) for the VRFB anode, which was confirmed through a 13cycle test. In particular, at a high current density (160 mA/cm^2), the EE reached 82.03%, which is 6.2% higher than that of pristine GF electrode. In addition, the NTO-HGF electrodes exhibited high stability during long-term cycling tests up to 100 cycles in acidic electrolytes. These improvements in electrochemical performance were mainly due to (1) the NTO lamination layer on the heat-treated GF structure, which provided a sufficient effective contact area for V^{3+}/V^{2+} ions and electron transfer between the electrode and electrolyte; (2) the NTO lamination layer providing more oxygen-containing functional groups, which improved the hydrophilicity and catalytic activity of the NTO-HGF electrode; and (3) the high electrical conductivity of the Nb-doped TiO_2 lattice structure contributing to a faster charge transfer at the GF surface, which resulted in superior energy storage efficiency. These results verified that the HGF with an NTO lamination layer exhibits significant potential as a high-performance VRFB anode.

CRediT authorship contribution statement

Wen-Fei Liu: Conceptualization, Methodology, Investigation, Data curation, Writing – original draft. **Kue-Ho Kim**: Methodology, Investigation, Data curation. **Hyo-Jin Ahn**: Conceptualization, Supervision, Writing – review & editing.

Data Availability

Data will be made available on request.

Declaration of Competing Interest

The authors declare that they have no known competing financial interests or personal relationships that could have appeared to influence the work reported in this paper.

Acknowledgements

This research was supported by Basic Science Research Program through the National Research Foundation of Korea (NRF) funded by the Ministry of Education (NRF-2021R1A6A1A03039981) and Commercialization Promotion Agency for R&D Outcomes(COMPA) funded by the Ministry of Science and ICT(MSIT) (Mass production technology of 4,000 cm^2 scale carbon-coated metal components, 2021COMPA-106).

Appendix A. Supporting information

Supplementary data associated with this article can be found in the online version at doi:10.1016/j.jallcom.2023.170106.

References

[1] T. Li, F. Xing, T. Liu, J. Sun, D. Shi, H. Zhang, X. Li, Cost, performance prediction and optimization of a vanadium flow battery by machine-learning, Energy Environ. Sci. 13 (2020) 4353–4361.
[2] J. Xue, Y. Jiang, Z. Zhang, T. Zhang, C. Han, Y. Liu, Z. Chen, Z. Xie, L. Zhanggao, L. Dai, L. Wang, Z. He, A novel catalyst of titanium boride toward V^{3+}/V^{2+} redox reaction for vanadium redox flow battery, J. Alloy. Compd. 875 (2021) 159915.
[3] M. Skyllas-Kazacos, D. Kasherman, D.R. Hong, M. Kazacos, Characteristics and performance of 1 kW UNSW vanadium redox battery, J. Power Sources 35 (1991) 399–404.
[4] Y.K. Zeng, X.L. Zhou, L. An, L. Wei, T.S. Zhao, A high-performance flow-field structured iron-chromium redox flow battery, J. Power Sources 324 (2016) 738–744.
[5] R. Kim, S. Yuk, J.H. Lee, C. Choi, S. Kim, J. Heo, H.T. Kim, Scaling the water cluster size of Nafion membranes for a high performance Zn/Br, Redox Flow. Battery, J. Membr. Sci. 564 (2018) 852–858.
[6] M. Skyllas-Kazacos, G. Kazacos, G. Poon, H. Verseema, Recent advances with UNSW vanadium-based redox flow batteries, Int. J. Energy Res. 34 (2010) 182–189.
[7] R.M. Dell, D.A.J. Rand, Energy storage—a key technology for global energy sustainability, J. Power Sources 100 (2001) 2–17.
[8] Z. González, A. Sánchez, C. Blanco, M. Granda, R. Menéndez, R. Santamaría, Enhanced performance of a Bi-modified graphite felt as the positive electrode of a vanadium redox flow battery, Electrochem. Commun. 13 (2011) 1379–1382.
[9] C. Wang, H. Song, C. Yu, Z. Ullah, Z. Guan, R. Chu, Y. Zhang, L. Zhao, Q. Li, L. Liu, Iron single-atom catalyst anchored on nitrogen-rich MOF-derived carbon nanocage to accelerate polysulfide redox conversion for lithium sulfur batteries, J. Mater. Chem. A 8 (2020) 3421–3430.

[10] C. Wang, R. Chu, Z. Guan, Z. Guan, Z. Ullah, H. Song, Y. Zhang, C. Yu, L. Zhao, Q. Li, L. Liu, Tailored polyimide as positive electrode and polyimide-derived carbon as negative electrode for sodium ion full batteries, Nanoscale 12 (2020) 4729–4735.
[11] L. Zhao, Y. Ning, Q. Dong, Z. Ullah, P. Zhu, S. Zheng, G. Xia, S. Zhu, Q. Li, L. Liu, Longer cycle life and higher discharge voltage of a small molecular indanthrone resulting from the extended conjugated framework, J. Power Sources 556 (2023) 232518.
[12] C. Wang, Q. Ji, R. Chu, Z. Ullah, M. Zheng, X. Dong, Y. Sun, Q. Li, L. Liu, High-Performance PDB organic cathodes reinforced by 3D flowerlike carbon for lithium-/sodium-ion batteries, ACS Appl. Energy Mater. 4 (2021) 12641–12648.
[13] R. Chu, H. Song, Z. Ullah, Z. Guan, Y. Zhang, L. Zhao, M. Chen, W. Li, Q. Li, L. Liu, ZIF-8 derived nitrogen-doped carbon composites boost the rate performance of organic cathodes for sodium ion batteries, Electrochim. Acta 362 (2020) 137115.
[14] Y.C. Chang, Y.C. Shih, J.Y. Chen, G.Y. Lin, N.Y. Hsu, Y.S. Chou, C.H. Wang, High efficiency of bamboo-like carbon nanotubes on functionalized graphite felt as electrode in vanadium redox flow battery, RSC Adv. 6 (2016) 102068–102075.
[15] T.X.H. Le, M. Bechelany, M. Cretin, Carbon felt based-electrodes for energy and environmental applications: a review, Carbon 122 (2017) 564–591.
[16] T.X.H. Le, R. Esmilaire, M. Drobek, M. Bechelany, C. Vallicari, S. Cerneaux, A. Julbe, M. Cretin, Nitrogen-doped graphitized carbon electrodes for biorefractory pollutant removal, J. Phys. Chem. C. 121 (2017) 15188–15197.
[17] D.J. Suárez, Z. González, C. Blanco, M. Granda, R. Menéndez, R. Santamaría, Graphite felt modified with bismuth nanoparticles as negative electrode in a vanadium redox flow battery, ChemSusChem 7 (2014) 914–918.
[18] H.R. Jiang, W. Shyy, L. Zeng, R.H. Zhang, T.S. Zhao, Highly efficient and ultrastable boron-doped graphite felt electrodes for vanadium redox flow batteries, J. Mater. Chem. A 6 (2018) 13244–13253.
[19] S.J. Yoon, S. Kim, D.K. Kim, S. So, Y.T. Hong, R. Hempelmann, Ionic liquid derived nitrogen-doped graphite felt electrodes for vanadium redox flow batteries, Carbon 166 (2020) 131–137.
[20] H.J. Lee, H. Kim, Graphite felt coated with dopamine-derived nitrogen-doped carbon as a positive electrode for a vanadium redox flow battery, J. Electrochem. Soc. 162 (2015) A1675–A1681.
[21] H. Abedi, M. Mehrpooya, Synthesis of three-metal layered double hydroxide and dual doped graphene oxide composite as a novel electrocatalyst for oxygen reduction reaction, J. Alloy. Compd. 875 (2021) 160047.
[22] D.M. Kabtamu, J.Y. Chen, Y.C. Chang, C.H. Wang, Electrocatalytic activity of Nb-doped hexagonal WO_3 nanowire-modified graphite felt as a positive electrode for vanadium redox flow batteries, J. Mater. Chem. A 4 (2016) 11472–11480.
[23] H.M. Tsai, S.J. Yang, C.C.M. Ma, X. Xie, Preparation and electrochemical activities of iridium-decorated graphene as the electrode for all-vanadium redox flow batteries, Electrochim. Acta 77 (2012) 232–236.
[24] R.H. Huang, C.H. Sun, T.M. Tseng, W.K. Chao, K.L. Hsueh, F.S. Shieu, Investigation of active electrodes modified with platinum/multiwalled carbon nanotube for vanadium redox flow battery, J. Electrochem. Soc. 159 (2012) A1579.
[25] P. Han, H. Wang, Z. Liu, X. Chen, W. Ma, J. Yao, Y. Zhu, G. Cui, v Graphene oxide nanoplatelets as excellent electrochemical active materials for VO^{2+}/VO_2+ and V^{2+}/V^{3+} redox couples for a vanadium redox flow battery, Carbon 49 (2011) 693–700.
[26] X.G. Li, K.L. Huang, S.Q. Liu, T.A.N. Ning, L.Q. Chen, Characteristics of graphite felt electrode electrochemically oxidized for vanadium redox battery application, Trans. Nonferrous Met. Soc. China 17 (2007) 195–199.
[27] M. Park, Y.J. Jung, J. Kim, H.I. Lee, J. Cho, Synergistic effect of carbon nanofiber/nanotube composite catalyst on carbon felt electrode for high-performance all-vanadium redox flow battery, Nano Lett. 13 (2013) 4833–4839.
[28] Y. Shi, S. Zhang, W. Li, S. Kong, J. Xin, Y. Yang, X. Zhang, X. Wang, Simultaneous removal of Cr(VI) and phenol in a dual-chamber photocatalytic microbial fuel with $NiCo_2O_4/MoS_2$/GF photocathode, J. Alloy. Compd. 942 (2023) 168993.
[29] B.-R. Koo, D.-H. Oh, H.-J. Ahn, Influence of Nb-doped TiO_2 blocking layers as a cascading band structure for enhanced photovoltaic properties, Appl. Surf. Sci. 433 (2018) 27–34.
[30] D.-Y. Shin, B.-R. Koo, H.-J. Ahn, Lithium storage kinetics of highly conductive F-doped SnO_2 interfacial layer on lithium manganese oxide surface, Appl. Surf. Sci. 499 (2020) 144057.
[31] K.-W. Sung, D.-Y. Shin, H.-J. Ahn, Boosting ultrafast Li storage kinetics of conductive Nb-doped TiO_2 functional layer coated on $LiMn_2O_4$, J. Alloy. Compd. 870 (2021) 159404.
[32] H. An, H.-J. Ahn, A change in morphology from anatase-TiO_2 nanoparticles to anatase-TiO_2 nanoflakes via electrospray, Mater. Lett. 81 (2012) 41–44.
[33] T. Hitosugi, H. Kamisaka, K. Yamashita, H. Nogawa, Y. Furubayashi, S. Nakao, N. Yamada, A. Chikamatsu, H. Kumigashira, M. Oshima, Y. Hirose, T. Shimada, T. Hasegawa, Electronic band structure of transparent conductor: Nb-doped anatase TiO_2, Appl. Phys. Express 1 (2008) 111203.
[34] Z. He, Y. Jiang, Y. Li, J. Zhu, H. Zhou, W. Meng, L. Wang, L. Dai, Carbon layer-exfoliated, wettability-enhanced, SO_3H-functionalized carbon paper: A superior positive electrode for vanadium redox flow battery, Carbon 127 (2018) 297–304.
[35] G.-H. An, Y.-G. Lee, H.-J. Ahn, Multi-active sites of iron carbide nanoparticles on nitrogen@cobalt-doped carbon for a highly efficient oxygen reduction reaction, J. Alloy. Compd. 746 (2018) 177–184.
[36] W. Li, Z. Zhang, Y. Tang, H. Bian, T.W. Ng, W. Zhang, C.S. Lee, Graphene-nanowall-decorated carbon felt with excellent electrochemical activity toward VO^{2+}/VO_2^+ couple for all vanadium redox flow battery, Adv. Sci. 3 (2016) 1500276.
[37] H.H. Kristoffersen, H.L. Neilson, S.K. Buratto, H. Metiu, Stability of V_2O_5 supported on titania in the presence of water, bulk oxygen vacancies, and adsorbed oxygen atoms, J. Phys. Chem. C. 121 (2017) 8444–8451.
[38] P. Han, Y. Yue, Z. Liu, W. Xu, L. Zhang, H. Xu, S. Dong, G. Cui, Graphene oxide nanosheets/multi-walled carbon nanotubes hybrid as an excellent electrocatalytic material towards VO^{2+}/VO_2^+ redox couples for vanadium redox flow batteries, Energy Environ. Sci. 4 (2011) 4710–4717.
[39] Y. Long, M. Ding, C. Jia, Application of nanomaterials in aqueous redox flow batteries, ChemNanoMat 7 (2021) 699–712.
[40] Y. Lv, Y. Yang, J. Gao, J. Li, W. Zhu, L. Dai, Y. Liu, L. Wang, Z. He, Controlled synthesis of carbon nanonetwork wrapped graphite felt electrodes for high-performance vanadium redox flow battery, Electrochim. Acta 431 (2022) 141135.
[41] D.M. Kabtamu, A.W. Bayeh, T.C. Chiang, Y.C. Chang, G.Y. Lin, T.H. Wondimu, S.K. Su, C.H. Wang, $TiNb_2O_7$ nanoparticle-decorated graphite felt as a high-performance electrode for vanadium redox flow batteries, Appl. Surf. Sci. 462 (2018) 73–80.
[42] K.-H. Kim, B.-R. Koo, H.-J. Ahn, Sheet resistance dependence of fluorine-doped tin oxide films for high-performance electrochromic devices, Ceram. Int. 44 (2018) 9408–9413.
[43] Y. Xiang, W.A. Daoud, Binary $NiCoO_2$-modified graphite felt as an advanced positive electrode for vanadium redox flow batteries, J. Mater. Chem. A 7 (2019) 5589–5600.